Synthesis, Phase Behavior, and Curing Studies of Bisacetylene Rigid-Rod Thermosets

Elliot P. Douglas,* David A. Langlois, and Brian C. Benicewicz

Polymers and Coatings Group, Los Alamos National Laboratory, Los Alamos, New Mexico 87545

Received May 16, 1994. Revised Manuscript Received July 25, 1994®

We have synthesized a series of rigid-rod bisacetylene thermosets from 4-ethynylbenzoyl chloride and various substituted dihydroxy aromatic compounds. The resulting thermoset monomers can show no melting transition, a crystal-to-nematic transition, or a crystal-to-isotropic transition, depending on the substituent and the central aromatic group. Molecular modeling was used to explain this phase behavior. The observed transitions are determined by a balance between molecular linearity, substituent bulkiness, and intermolecular interactions. Optical microscopy was used to observe phase behavior during thermal curing. Nematic monomers can be cured in the liquid-crystalline melt to give a cross-linked solid that retains the nematic order. Qualitatively, the phase behavior during cure follows a generalized nonequilibrium phase diagram for liquid-crystal thermosets. Quantitative measurements of the curing kinetics were performed using Raman spectroscopy. Comparisons between isomeric compounds which melted into either a nematic phase or an isotropic phase show that the curing reaction occurs faster in the nematic phase by up to 126%.

Introduction

Over the past 20 years liquid-crystal polymers have been extensively investigated.[1,2] Due to their rigidity and anisotropy they exhibit outstanding physical properties, for example, high strength, high modulus, and good barrier properties. In particular, a great deal of attention has been focused on their use as fibers for advanced composites.

In comparison, little attention has been given to the use of liquid-crystalline materials as matrix materials for composites. Compared to high-performance fibers, conventional matrix materials exhibit poor mechanical properties, usually being very brittle and having low strength. Our interest in liquid-crystal thermosets (LCTs) has been as improved matrix materials for composite and other structural applications.

The concept of LCTs is well established and has been described previously.[3–5] Briefly, an LCT consists of a mesogenic central core to which conventional cross-linking end groups are attached. A schematic diagram of this concept is shown in Figure 1. The end groups can then be cured using conventional methods to give a cross-linked network that retains the order of the liquid-crystalline phase.

The first description of liquid-crystalline networks was given by deGennes.[6] A few reports in the early 1970s described the first experimental work on LCTs.[3,7]

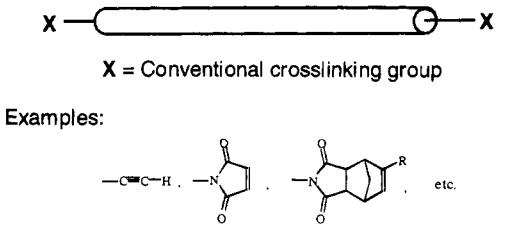

Figure 1. Schematic diagram of the liquid-crystal thermoset concept.

Interest in LCTs was revived in the early 1980s with the publication of several patents.[8–12] Since then a number of publications have addressed the synthesis and thermal behavior of LCTs.[13–18] There have been relatively few reports on the physical properties of these materials. It has been reported that some LCTs show very low shrinkage upon curing[16] and that macroscopically oriented LCTs exhibit an anisotropic coefficient of thermal expansion.[17,18]

Previous reports from our laboratory have described ester and amide LCTs with bismaleimide and bisnadimide end groups.[4,5] In this paper we extend this work to ester-based bisacetylene thermosets whose general structure is shown in Figure 2. These thermo-

® Abstract published in *Advance ACS Abstracts,* September 15, 1994.

(1) *Polymer Liquid Crystals*; Ciferri, A., Krigbaum, W. R., Meyer, R. B., Eds.; Academic Press: New York, 1982.
(2) *Liquid Crystallinity in Polymers: Principles and Fundamental Properties*; Ciferri, A., Ed.; VCH Publishers: New York, 1991.
(3) Clough, S. B.; Blumstein, A.; Hsu, E. C. *Macromolecules* **1976,** *9,* 123.
(4) Hoyt, A. E.; Benicewicz, B. C. *J. Polym. Sci., Part A: Polym. Chem.* **1990,** *28,* 3403.
(5) Hoyt, A. E.; Benicewicz, B. C. *J. Polym. Sci., Part A: Polym. Chem.* **1990,** *28,* 3417.
(6) deGennes, P. G. *Phys. Lett. A* **1969,** *28A,* 725.
(7) Liebert, L.; Strzelecki, L. *Chim. Macromol.* **1973,** *276,* 647.
(8) Conciatori, A. B.; Choe, E. W.; Farrow, G. 1984, U.S. Patent 4,440,945.
(9) Conciatori, A. B.; Choe, E. W.; Farrow, G. 1984, U.S. Patent 4,452,993.
(10) Conciatori, A. B.; Choe, E. W.; Farrow, G. 1985, U.S. Patent 4,514,553.
(11) Calundann, G. W.; Rasoul, H. A. A.; Hall, H. K. 1987, U.S. Patent 4,654,412.
(12) Stackman, R. W. 1987, U.S. Patent 4,683,327.
(13) Litt, M. H.; Whang, W.; Yen, K.; Qian, X. *J. Polym. Sci. Part A: Polym. Chem.* **1993,** *31,* 183.
(14) Melissaris, A. P.; Litt, M. H. *Macromolecules* **1994,** *27,* 883.
(15) Melissaris, A. P.; Litt, M. H. *Macromolecules* **1994,** *27,* 888.
(16) Melissaris, A. P.; Litt, M. H. *Macromolecules,* in press.
(17) Barclay, G. G.; Ober, C. K.; Papathomas, K. I.; Wang, D. W. *Macromolecules* **1992,** *25,* 2947.
(18) Barclay, G. G.; McNamee, S. G.; Ober, C. K.; Papathomas, K. I.; Wang, D. W. *J. Polym. Sci., Part A: Polym. Chem.* **1992,** *30,* 1845.

0897-4756/94/2806-1925$04.50/0

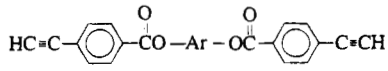

Figure 2. General structure of the bisacetylene thermosets. –Ar– is an aromatic group.

sets are similar to ones described previously by Melissaris and Litt.[16] However, where their main interest was solid-state polymerization of thermosets that do not exhibit a melting transition, our main interest in this paper is describing the phase behavior of thermosets that melt below the solid-state polymerization temperature. We use thermal analysis, microscopy, and molecular modeling to describe the effect of molecular structure on the phase behavior. In addition, we have performed extensive kinetic analysis to compare the cure rates of liquid-crystalline and non-liquid-crystalline thermosets. While there have been some comparisons of this type reported,[19,20] our analysis provides the first quantitative comparison between reactions in two different phases at the same curing temperature.

Experimental Section

Synthesis. The bisacetylene monomers in Table 1 were synthesized by the reaction of the appropriate diol with 4-ethynylbenzoyl chloride. The 4-ethynylbenzoyl chloride was synthesized according to the method of Melissaris and Litt.[21] All monomers were synthesized using the procedure of Melissaris and Litt.[16] Monomers **1**, **2**, **3**, **7**, and **8** have been reported previously.[16]

Monomer 4: Recrystallized from acetonitrile. ^{1}H NMR (DMF-d_7) δ 8.21 (m, 4H), 8.04 (s, 1H), 7.78 (m, 4H), 6.81 (s, 1H), 4.48 (s, 2H), 3.98 (s, 3H), 3.72 (s, 3H). ^{13}C NMR (DMF-d_7) δ 164.9, 164.2, 163.1, 156.6, 151.1, 137.8, 133.0, 130.8, 130.2, 129.5, 128.4, 128.2, 126.1, 115.7, 109.8, 84.0, 83.8, 83.3, 83.2, 57.3, 52.3. Anal. Calcd for $C_{27}H_{18}O_7$: C, 71.36; H, 3.99; O, 24.64. Found: C, 71.05; H, 4.15.

Monomer 5: Recrystallized from DMF/H_2O. ^{1}H NMR (DMF-d_7) δ 8.22 (d, 4H), 7.78 (d, 4H), 7.30 (m, 6H), 4.50 (s, 2H), 2.13 (s, 6H). ^{13}C NMR (DMF-d_7) δ 164.9, 150.9, 139.1, 138.2, 133.0, 131.1, 130.7, 130.2, 128.2, 123.7, 119.9, 83.9, 83.3, 19.9. Anal. Calcd for $C_{32}H_{22}O_4$: C, 81.69; H, 4.71; O, 13.60. Found: C, 81.40; H, 4.84.

Monomer 6: Recrystallized from acetonitrile. ^{1}H NMR (DMF-d_7) δ 8.24 (m, 4H), 7.78 (d, 4H), 7.28 (s, 2H), 4.50 (s, 2H), 2.20 (s, 6H). ^{13}C NMR (DMF-d_7) δ 164.7, 147.8, 133.1, 131.3, 130.8, 129.9, 128.3, 121.1, 83.9, 83.2, 13.0. Anal. Calcd for $C_{26}H_{18}O_4$: C, 79.17; H, 4.60; O, 16.23. Found: C, 79.13; H, 4.56.

Monomer 9: Recrystallized from ethanol. ^{1}H NMR (DMF-d_7) δ 8.20 (m, 4H), 7.78 (m, 4H), 7.44 (d, 1H), 7.35 (d, 1H), 4.49 (s, 2H), 3.88 (s, 3H). ^{13}C NMR (DMF-d_7) δ 164.8, 164.3, 162.7, 152.6, 150.3, 138.2, 133.0, 130.7, 130.1, 129.8, 128.3, 123.9, 114.4, 108.2, 83.8, 83.2, 56.7. Anal. Calcd for $C_{25}H_{16}O_5$: C, 75.75; H, 4.07; O, 20.18. Found: C, 75.54; H, 4.01.

Monomer 10: Recrystallized from acetonitrile. ^{1}H NMR (DMF-d_7) δ 8.24 (m, 2H), 8.10 (m, 2H), 7.78 (d, 2H), 7.70 (d, 2H), 7.60 (m, 5H), 7.38 (m, 3H), 4.48 (d, 2H). ^{13}C NMR (DMF-d_7) δ 164.8, 149.7, 146.2, 137.1, 136.5, 133.0, 130.7, 130.1, 129.7, 129.5, 129.1, 128.6, 128.3, 125.2, 124.6, 122.8, 83.9, 83.2. Anal. Calcd for $C_{30}H_{18}O_4$: C, 81.44; H, 4.10; O, 14.46. Found: C, 81.49; H, 4.20.

Monomer 11: Recrystallized from acetonitrile/H_2O. ^{1}H NMR (DMF-d_7) δ 8.22 (m, 2H), 8.02 (m, 2H), 7.77 (m, 2H), 7.68 (m, 3H), 7.51 (d, 2H), 4.61 (t, 2H), 4.50 (s, 1H), 4.42 (s, 1H), 3.20 (t, 2H). ^{13}C NMR (DMF-d_7) δ 165.8, 164.1, 146.3, 139.3, 133.1, 132.8, 131.3, 130.8, 130.1, 129.8, 129.3, 128.6, 127.6, 126.7, 124.8, 84.1, 83.4, 83.2, 65.9, 34.5. Anal. Calcd for $C_{26}H_{17}ClO_4$: C, 72.82; H, 4.00; Cl, 8.27; O, 14.92. Found: C, 72.68; H, 4.02; Cl, 8.29.

Monomer 12: Recrystallized from acetonitrile. ^{1}H NMR (DMF-d_7) δ 8.23 (m, 4H), 7.77 (m, 6H), 7.48 (m, 1H), 4.50 (d, 2H). ^{13}C NMR (DMF-d_7) δ 164.5, 163.8, 151.0, 148.1, 133.0, 131.2, 130.8, 129.6, 129.1, 128.7, 128.4, 124.4, 122.2, 119.3, 84.2, 84.0, 83.1. Anal. Calcd for $C_{24}H_{13}ClO_4$: C, 71.92; H, 3.27; Cl, 8.85; O, 15.97. Found: C, 71.55; H, 3.25; Cl, 8.83.

Monomer 13: Recrystallized from acetonitrile. ^{1}H NMR (DMF-d_7) δ 8.19 (m, 4H), 7.75 (m, 4H), 7.21 (m, 3H), 4.48 (s,

Table 1. Structure and Thermal Transitions of Bisacetylene Monomers

monomer	–Ar–	name	endo (°C)	phase behavior	exo (°C)
1	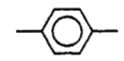	HQ	none (none)[a]	crystalline	211 (227)[b]
2	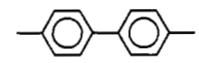	BP	none (none)	crystalline	217 (220)
3	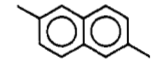	NA	none (none)	crystalline	207 (211)
4	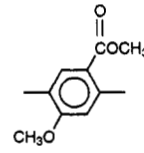	MOBHQ	none	crystalline	229
5	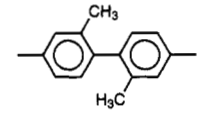	2MBP	168	k → n	182
6	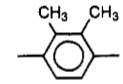	2MHQ	176	k → n	181
7	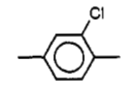	ClHQ	183 (173)	k → n	189 (218)
8	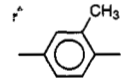	MHQ	164 (167)	k → n	178 (204)
9	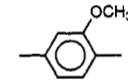	MeOHQ	154 k → n 164 n → i		178
10	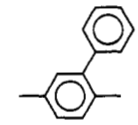	PHHQ	182	k → i	192
11	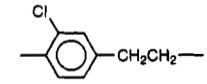	ClEtHQ	113	k → i	187
12	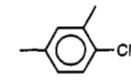	ClR	157	k → i	192
13	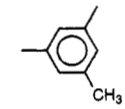	MR	177	k → i	194
14	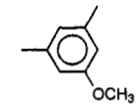	MeOR	139	k → i	185

[a] Melting temperatures as reported by Melissaris and Litt.[16] [b] Exotherm temperatures as reported by Melissaris and Litt.[16] Note that this work reports the exotherms as extrapolated onset temperatures, while ref 16 reports them as peak maximum temperatures.

(19) Hoyle, C. E.; Kang, D.; Chawla, C. P.; Griffin., A. C. *Polym. Eng. Sci.* **1992**, *32*, 1490.
(20) Hoyle, C. E.; Chawla, C. P.; Kang, D.; Griffin, A. C. *Macromolecules* **1993**, *26*, 758.
(21) Melissaris, A. P.; Litt, M. H. *J. Org. Chem.* **1992**, *57*, 6998.

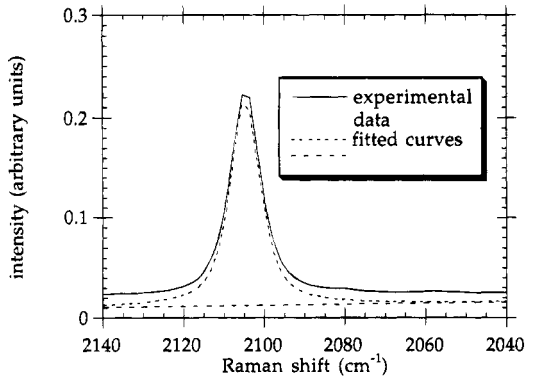

Figure 3. Example of the curve fitting of the Raman spectra for quantitative cure analysis. The experimental data have been shifted vertically for clarity.

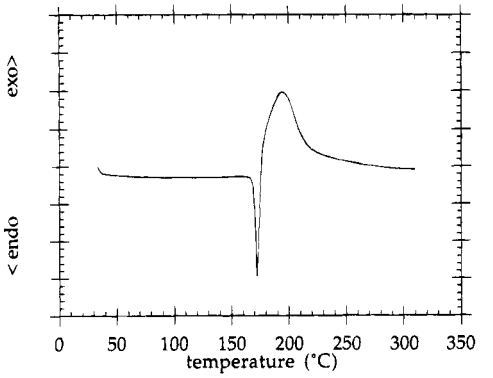

Figure 4. DSC curve for MHQ.

2H), 2.44 (s, 3H). ^{13}C NMR (DMF-d_7) δ 164.7, 152.0, 141.4, 133.0, 130.7, 128.3, 120.8, 113.9, 83.9, 83.2, 21.1. Anal. Calcd for $C_{25}H_{16}O_4$: C, 78.94; H, 4.24; O, 16.82. Found: C, 78.89; H, 4.27.

Monomer 14: Recrystallized from acetonitrile. ^{1}H NMR (DMF-d_7) δ 8.18 (m, 4H), 7.76 (m, 4H), 7.03 (m, 3H), 4.47 (s, 2H), 3.90 (s, 3H). ^{13}C NMR (DMF-d_7): δ 164.5, 161.7, 152.9, 133.0, 130.7, 130.0, 128.3, 109.1, 106.7, 83.9, 83.2, 56.4. Anal. Calcd for $C_{25}H_{16}O_5$: C, 75.75; H, 4.07; O, 20.18. Found: C, 75.46; H, 4.02.

Nuclear Magnetic Resonance Spectroscopy. NMR spectra were obtained on either a Bruker AC250 250 MHz spectrometer or a JEOL GSX-270 270 MHz spectrometer. All measurements were performed using DMF-d_7 as the solvent.

Thermal Analysis. Differential scanning calorimetry (DSC) was performed using a Polymer Laboratories DSC operated at a heating rate of 20 °C/min. Transition temperatures are reported as the extrapolated onset. The phases were determined using optical microscopy. Microscopy was performed using a Zeiss Universal Microscope equipped with a Linkam hot stage. Samples were placed between glass cover slips on the silver block of the hot stage. The heating rate for microscopy was 5 °C/min, and the samples were observed under crossed polars to determine the phases. In some cases the samples were held isothermally in the microscope to observe the phase behavior as a function of cure time. In these cases the samples were heated at 100 °C/min to the desired temperature and then held isothermally.

Molecular Modeling. Molecular modeling was done using the commercial software PCModel available from Serena Software. This software uses the MMX force field.[22] For our calculations the π–π interactions were calculated using the reduced Hartree–Fock and Huckel approximations.

Curing Analysis. Samples for curing analysis were prepared by placing the sample on a preheated coverslip on a hot plate and allowing to cure isothermally for the desired time. In this way curing times ranging from 15 s to 10 min could be measured. In a few cases longer curing times were also measured. For these measurements the sample was placed in an NMR tube and cured isothermally in an oven under vacuum.

After curing the amount of reaction that had taken place was measured using Raman spectroscopy. Spectra were measured using a Nicolet Raman 910 spectrometer using a Nd:YAG laser operating at 300 mW. The spectra were obtained by averaging over 100 scans.

Spectra were first normalized to the absorbance of the carbonyl band at 1735 cm^{-1}, and then the absorbance of the acetylene band at 2108 cm^{-1} was determined. Absorbances were calculated by fitting the desired absorbance to a single peak of mixed Gaussian and Lorentzian character and a baseline. An example of the fit is given in Figure 3, where the experimental data has been shifted vertically for clarity. Since both the carbonyl and the acetylene absorbances were single isolated peaks, there were no fixed parameters in the peak fitting procedure. The amount of cure was determined from the acetylene absorbances by

$$\% \text{ cure} = 100(1 - A_t/A_0)$$

where A_t is the absorbance at time t and A_0 is the initial absorbance of the uncured material. For quantitative analysis of the cure rate only the data taken for cure times of 90 s and less was used (see Results and Discussion). For those times three points were measured at each time and temperature and averaged.

We found that for the uncured crystalline material A_0 was actually less than A_t at t = 15 s. Therefore, A_0 for our calculations was actually the absorbance measured for a sample that had been melted and then immediately removed from the hot plate. For each material several samples were melted at several temperatures, and the sample which gave the highest value of A_0 was used for the calculation. The error resulting from using different values of A_0 determined in this fashion was less than the error resulting from averaging three samples for each point.

Results and Discussion

Thermal Behavior. Thermal transitions for the bisacetylene thermosets were investigated using differential scanning calorimetry (DSC). A typical DSC trace is shown in Figure 4 for compound MHQ. It shows the general characteristics of a melting endotherm followed by a polymerization exotherm. The transition temperatures for all compounds are shown in Table 1. Depending on the central aromatic group, the thermosets showed one, two, or no melting transitions. A more detailed discussion of the differences will be given later. We note that some of the compounds listed in Table 1 have been previously investigated by Litt.[16] We include those compounds here for completeness and note that our results agree with the previous work.

The phase behavior of the thermosets was determined by examining the samples in an optical microscope under crossed polars while being heated on a hot stage. The phases determined are also listed in Table 1. It is well recognized that one requirement for liquid crystallinity is collinearity of segments of the molecule.[23] We have used molecular modeling to determine whether the substituents result in a change in conformation, causing the difference in phase behavior.

Molecular modeling was done to determine the low-energy conformation of isolated molecules. The results

(22) Gajewski, J. J.; Gilbert, K. E.; McKelvey, J. in *Advances in Molecular Modeling, Volume 2* ; Liotta, D., ed.; JAI Press: Greenwich, CT, 1990, p 65.

(23) Irwin, R. S.; Vorpagel, E. R. *Macromolecules* **1993**, *26*, 3391.

Table 2. Minimum Energy Conformations[a] (deg)

material	ψ_1	ψ_2	θ_y	θ_z
HQ syn	42.7	−41.4	1.6	3.0
HQ anti	−40.5	−41.0	13.6	7.9
MOBHQ	55.1	−120.3	15.9	15.1
2MHQ	51.6	−65.9	0.4	5.5
ClHQ	45.4	−76.5	0.8	5.3
MHQ	43.8	−66.0	0.0	6.7
MeOHQ	44.4	−55.9	0.0	4.9
PHHQ	43.4	−58.1	1.6	4.9
ClEtHQ	67.4		45.0	35.1
ClR	−136.0	66.2	39.4	51.8
MR	51.3	44.7	46.5	49.5
MeOR	45.8	44.8	55.2	57.1

[a] See Figure 5 for definition of angles.

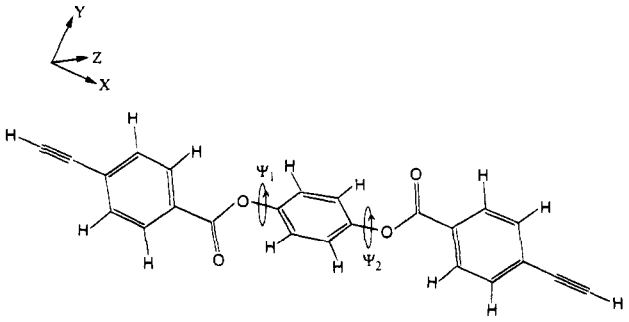

Figure 5. Minimum energy conformation for thermoset HQ. The torsional angles Ψ_1 and Ψ_2 refer to the angles between the central ring and the ester carbonyl. The axes define the angles θ_y and θ_z in Table 2. If one acetylene group is placed along the x axis, then the other acetylene group makes an angle θ_y with the x axis in the $x-y$ plane and an angle θ_z with the x axis in the $x-z$ plane.

for the unsubstituted HQ thermoset are shown in Figure 5. The conformation is one in which the two end rings are tilted at an angle of approximately 40° with respect to the central ring. This conformation results from the balance between π conjugation and steric hindrance between the carbonyl and the hydrogen on the central ring ortho to the ester linkage. This is similar to the conformation of poly(*p*-phenylene terephthalamide) in its crystalline form.[24]

Previous calculations on amides have shown that substituents can greatly affect the torsional angle between rings, resulting in an overall tilted conformation for the molecule.[23] The effect of the substituents on these torsional angles and the overall tilt of the molecules is given in Table 2. In all cases the substituents were added to the structure shown in Figure 5 and then reminimized. In those cases where there was only one substituent on the central ring, that substituent was artificially placed on the side closer to the ester carbonyl prior to reminimization in order to maximize the effect of the substituent during the minimization procedure.

The values for tilt in Table 2 give the angles that a line drawn from the acetylene carbon to the ester carbon of each of the end rings make with each other both in the plane of the paper and out of the plane of the paper (see Figure 5). The results show that in some cases tilt can explain the phase behavior. Clearly the resorcinol-based materials (MR, ClR, MeOR) and ClEtHQ have large tilts resulting from the resorcinol linkage and the ethyl linkage, respectively, causing an isotropic melt to form. Also, it appears that in some cases the tilt out of the plane is smallest for the materials that do not melt and larger for those that are liquid crystalline. For example, for HQ in the syn conformation the tilt is 3.0°, while for MHQ it is 6.7°. However, in other cases this trend breaks down. For example, HQ in the anti conformation has a tilt of 7.9°, and the largest tilt for the hydroquinone-based materials occurs for MOBHQ, which does not show any melting transition. Also, PHHQ, which is isotropic, has less tilt than MHQ, which is liquid crystalline. Thus we must look to additional factors to explain the phase behavior.

Table 3. Molecular Volumes of Minimum Energy Conformations

material	molecular vol (Å^3)	substituent vol (Å^3)[a]
HQ	470	
MOBHQ	582	112
2MHQ	525	55
ClHQ	492	22
MHQ	499	29
MeOHQ	511	41
PHHQ	580	110

[a] Determined by subtracting the molecular volume of HQ from the molecular volume for each of the materials with the substituents.

Another factor which can affect phase behavior is packing of the molecules. In particular, steric hindrance due to bulky side groups can greatly affect phase behavior. We have calculated the molecular volumes of the minimized structures in order to compare the effect of substituents of different sizes. The results are given in Table 3. The last column in Table 3 shows the difference in volume between the unsubstituted thermoset and the substituted thermoset. This difference is assumed to be due entirely to the volume of the substituent.

For the most part, differences between isotropic and nematic thermosets can be explained on the basis of molecular volume. In general, Table 3 shows that thermosets that do not melt have a substituent volume of 20−30 Å^3, those that are liquid crystalline have a substituent volume of 20−60 Å^3, and those that are isotropic have a substituent volume of 60 Å^3 or greater. Note that we can not determine from our analysis how the volumes of the substituents specifically affects packing, but the trend in substituent size appears to explain the behavior of our system.

There are two exceptions to this molecular volume argument. These are MOBHQ, which has the largest substituent volume but does not melt, and MeOHQ, which has a substituent volume of only 41 Å^3 but exhibits an isotropic phase. In both of these cases the substituents are very polar, and thus intermolecular interactions are likely to play a large role in determining packing. Kricheldorf et al. have previously shown that intermolecular interactions are largely responsible for the phase behavior of poly(ester imides).[25] In our system there appears to be a subtle balance among molecular linearity, substituent bulkiness, and interchain interactions which governs the phase behavior.

As has been described previously for liquid-crystal thermosets,[4,5] the bisacetylene monomers showing a nematic phase could be heated into that phase and cured to give a liquid-crystalline thermoset material.

(24) Northolt, M. G. *Eur. Polym. J.* **1974**, *10*, 799.

(25) Kricheldorf, H. R.; Schwarz, G.; Domschke, A.; Linzer, V. *Macromolecules* **1993**, *26*, 5161.

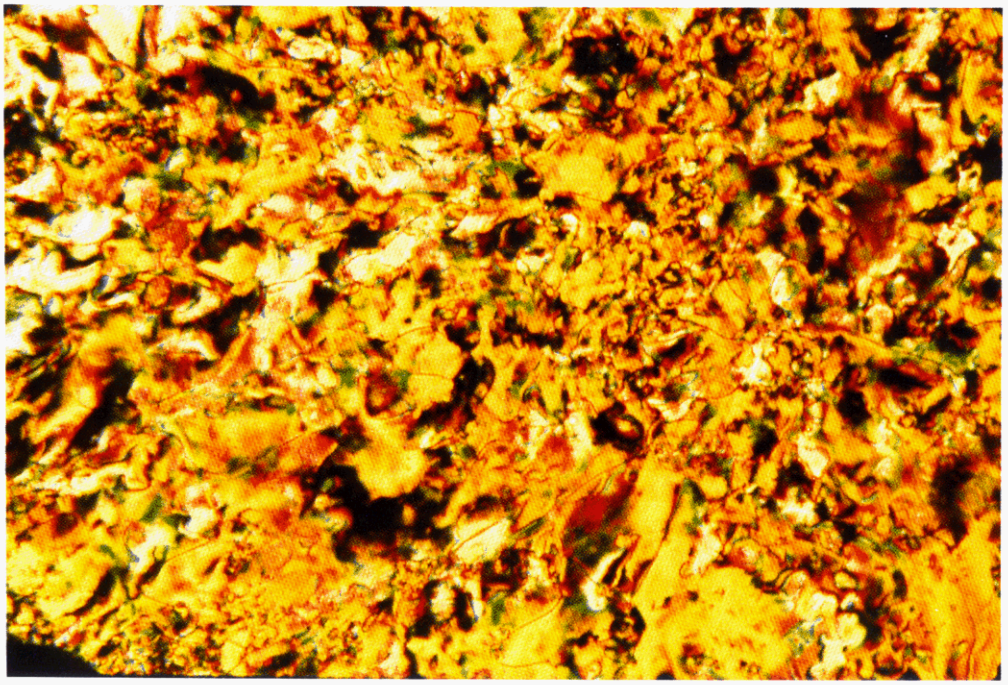

Figure 6. Polarized optical micrograph of MHQ melted and cured in the nematic phase. Magnification 80×.

Figure 6 shows a typical photograph of an LCT that has been cured in the nematic phase and cooled to room temperature.

The phase behavior of compound MeOHQ, which shows both crystal-to-nematic and nematic-to-isotropic transitions, is considerably more complicated. Figure 7 shows a series of photographs taken as the monomer was heated at 100 °C/min to 180 °C and then held there isothermally. The first two photographs in the series show what would be expected, namely, melting into the nematic phase followed by clearing to the isotropic phase. As curing then proceeds in the isotropic phase, there is an abrupt transition back to the nematic, followed by a final slower transition back to the isotropic. The final phase of the cured material is isotropic.

These changes in phase can be explained by considering a generalized phase diagram that has been previously used to describe the behavior of LCTs.[5] A slightly modified version of this phase diagram is shown in Figure 8. The change of MeOHQ from isotropic to nematic with cure occurs as the material proceeds from point A to point B on the phase diagram. This change occurs due to a change in the aspect ratio of the molecules as the cure reaction proceeds. Although initially in the isotropic state, as the reaction proceeds the molecules become longer and more rodlike, resulting in the formation of a nematic phase. This transition has also been seen previously in a nadimide-terminated LCT, although the time over which this transition occurred was much longer than for the bisacetylene due to the much slower kinetics of the nadimide curing reaction.[5]

The final slower change from the nematic phase back to the isotropic phase (parts d–h of Figure 7) is not explained by the phase diagram. Although we have no experimental data at this time upon which to base an explanation, we can offer two possibilities. The first is based on the fact that the phase diagram shows that the partially cured material will still show a clearing temperature, although at an elevated temperature compared to the uncured monomer. The large exotherm of polymerization (approximately 330 J/g) may heat the material to above this clearing temperature as the reaction occurs. Although the sample is held isothermally, the glass cover slip on which the sample rests may prevent efficient heat conduction to the silver block of the hot stage, allowing the increase in temperature.

A second explanation is that the cure chemistry drives the change back to the isotropic phase. Previous investigations of acetylene cure have shown the formation of two types of structures: linear diene chains and cyclic trimers.[26] The topology and rigidity of a benzene ring formed during a cyclotrimerization reaction would seem to favor the formation of an isotropic phase, since it is unlikely the mesogens would be able to align themselves in a liquid-crystalline phase when attached to a benzene ring. Thus, if cyclic trimers are formed in MeOHQ as it cures, the nematic melt would be transformed into an isotropic material. However, we note that Barclay et al. have reported the formation of liquid-crystalline thermosets based on dicyanates, which form triazine rings as the cross-linking sites.[17] This result seems to discount our explanation that the cure chemistry drives the formation of the isotropic phase. We are planning solid-state NMR studies to investigate the cure chemistry in more detail and determine if different structures are formed in the different phases.

Curing Studies. There have been many studies in the past which have examined the rate of reactions in liquid-crystal media.[27,28] Many of these earlier investigations have given conflicting results. For example, Amerik et al. have reported that *p*-methacryloylbenzoic acid polymerized faster in the liquid-crystalline phase

(26) Sefcik, M. D.; Stejskal, E. O.; McKay, R. A.; Schaefer, J. *Macromolecules* **1979**, *12*, 423.
(27) Barrall, E. M.; Johnson, J. F. *J. Macromol. Sci.—Rev. Macromol. Chem.* **1979**, *C17*, 137.
(28) Paleos, C. M. *Chem. Soc. Rev.* **1985**, *14*, 45.

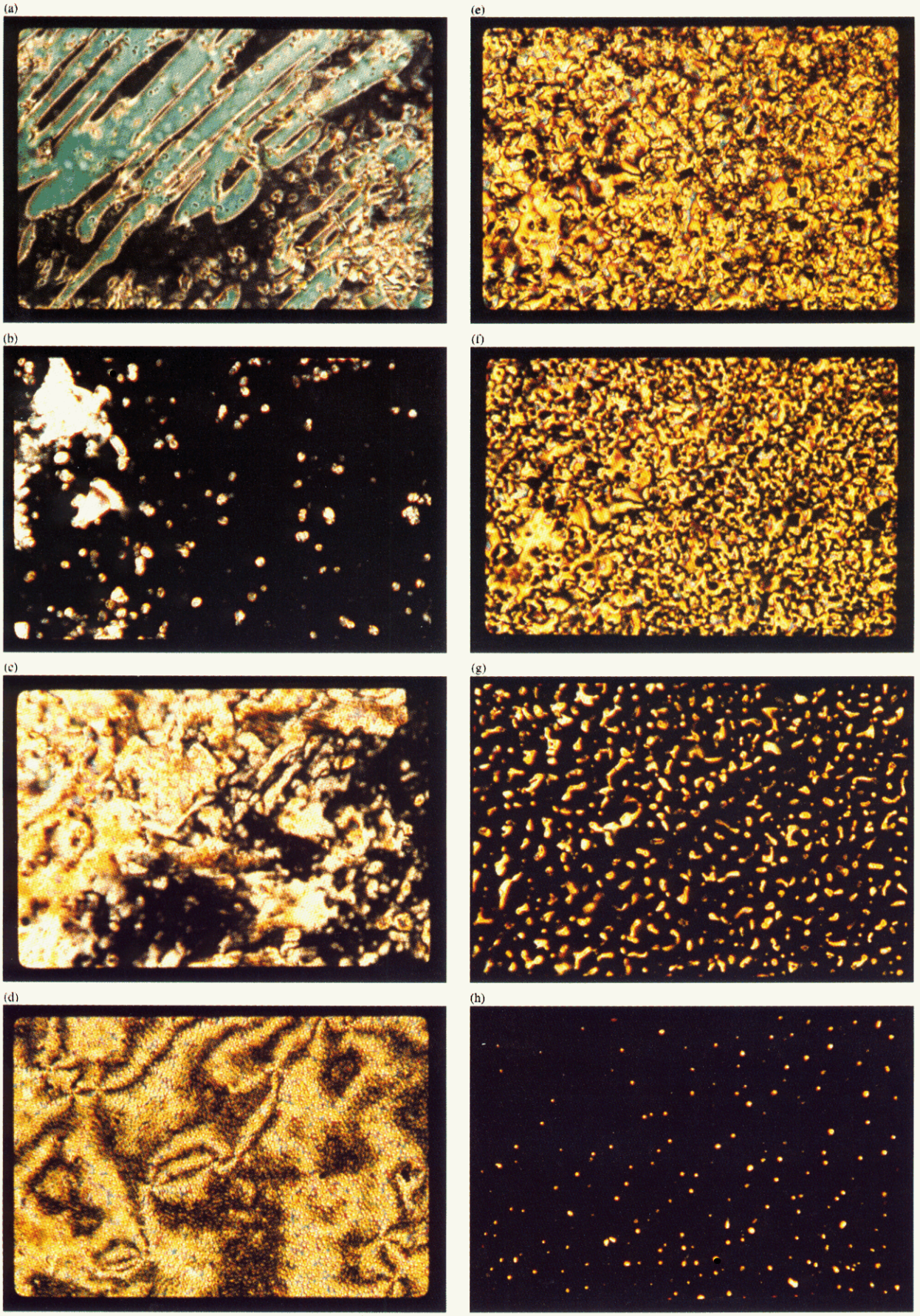

Figure 7. Series of polarized optical micrographs of MeOHQ as it is cured isothermally at 180 °C. Micrographs are taken at approximately (a) 5, (b) 10, (c) 15, (d) 30, (e) 45, (f) 60, (g) 90, and (h) 105 s after the first sign of melting. Magnification 45×.

than the isotropic phase.[29] On the other hand, Hsu and Blumstein reported that an Arrhenius plot for the reaction rate of a Shiff base showed no discontinuity at the nematic-to-isotropic transition, suggesting that

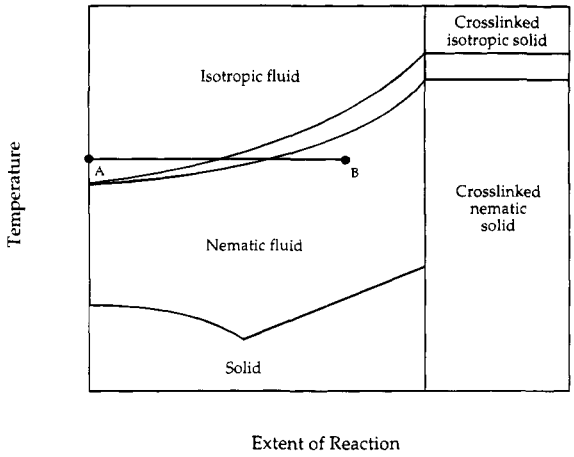

Figure 8. Nonequilibrium phase diagram describing the behavior of liquid-crystal thermosets. The path from A to B is the path taken by MeOHQ as shown by parts (a) and (b) of Figure 7.

there was no rate enhancement in the nematic phase.[30] Many of these conflicts, however, have resulted from a poor understanding of the phase in which the reaction occurred. For example, it appears that polymerization of *p*-methacryloylbenzoic acid may have actually occurred in a biphasic system.[27] More recently, Hoyle et al. have clearly shown a rate enhancement for a photochemical polymerization upon going from the isotropic to liquid-crystalline phases.[19,20] We have used Raman spectroscopy to follow the curing kinetics of liquid-crystalline and isotropic thermosets quantitatively.

The materials we have investigated are ClHQ, MHQ, MeOHQ, ClR, MR, and MeOR. These materials were chosen to provide a direct comparison between liquid-crystalline and isotropic materials of similar structure at the same curing temperature. This is in contrast to the recent work in which the same material was reacted at different temperatures in different phases.[19,20]

Previous work on bisacetylene curing has used predominately infrared spectroscopy,[31,32] although EPR,[33] NMR,[26,34] and Raman[32] measurements have also been used. As described in the Experimental Section, we have used Raman spectroscopy due to the presence of a single, resolved band at 2108 cm^{-1} assigned to the carbon−carbon triple bond which can easily be followed as a function of time.

The uncured and partially cured spectra for MeOHQ are shown in Figure 9. The decrease in the acetylene band at 2108 cm^{-1} can clearly be seen. The formation of new bands in the alkene region around 1550 cm^{-1} can also be seen. This increase is due to the formation of alkene species as the acetylene cure proceeds. The presence of two bands in this region is suggestive of the formation of two different species. This may reflect the formation of both polyene chains and cyclic trimers as has been previously reported.[26] However, we are not able to specifically identify how these bands in the

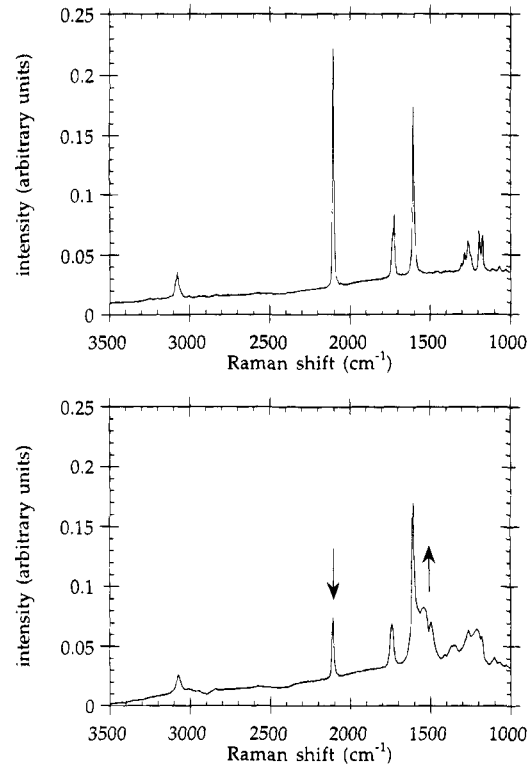

Figure 9. Normalized Raman spectra of MeOHQ uncured (top) and cured for 15 min at 180 °C (bottom). The arrows in the bottom figure show the changes that occur upon curing.

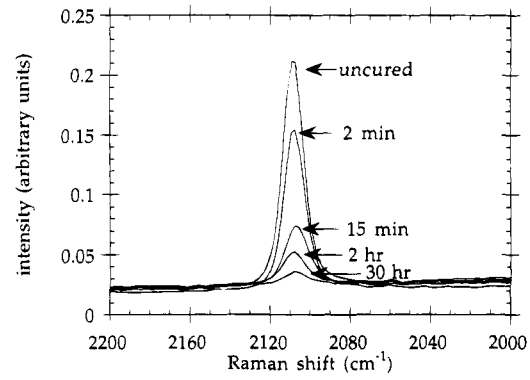

Figure 10. Decrease in acetylene band with time for MeOR cured at 180 °C. All curves have been normalized to the absorbance of the carbonyl band.

Raman spectra are related to molecular species. As stated in the previous section, we are planning solid-state NMR experiments to investigate this point further.

Figure 10 shows the disappearance of the acetylene band as a function of time. The areas of these bands were used to generate the kinetic curves as described in the Experimental Section. Examples of the resulting curves are shown in Figure 11. One can see from this data that the curing rate is extremely fast. At 220 °C a plateau is reached after approximately 100 s, at which point the materials are 80% cured. Even at 190 °C the thermosets are 60% cured after only 3 min of curing. We also note that the final level of cure is extremely high. A few samples have been measured after cure times up to 60 h, and it was found that the materials are over 90% cured after that time, even at the lower cure temperatures.

To compare the cure rates of liquid-crystalline and isotropic materials, the initial linear portions of the

(29) Amerik, Y. B.; Konstantinov, I. I.; Krentsel', V. A.; Malakhayev, Y. M. *Vysokomol. Soedin* **1967**, *9*, 2591.
(30) Hsu, E. C.; Blumstein, A. *J. Polym. Sci., Lett. Ed.* **1977**, *15*, 129.
(31) Levy, R. L.; Lee, C. Y. *Polym. Prepr.* **1982**, *23*, 181.
(32) Parker, S. F.; Lander, J. A.; Gerrard, D. L.; Bowley, H. J.; Hay, J. N. *High Perf. Polym.* **1989**, *1*, 311.
(33) Sandreczki, T. C.; Lee, C. Y. *Polym. Prepr.* **1982**, *23*, 185.
(34) Lind, A. C.; Lee, C. Y. *Polym. Prepr.* **1982**, *23*, 183.

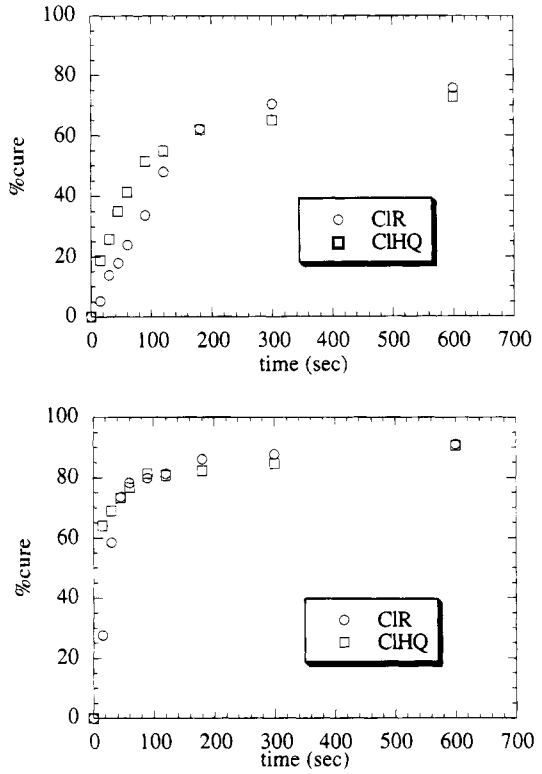

Figure 11. Curing curves for ClHQ and ClR cured at 190 (top) and 220 °C (bottom).

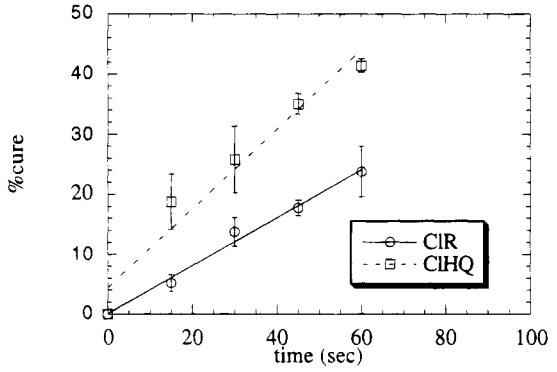

Figure 12. Initial linear region of curing curves used to determine the linear cure rates for ClR and ClHQ cured at 190 °C.

curing curves were used. Examples of this initial region are shown in Figure 12. We note that over this limited range the curves are fairly linear, and within 95% confidence limit all linear fits pass through the origin. A comparison of the slopes in Figure 12 clearly shows that the liquid-crystalline material cures faster than the comparable isotropic thermoset.

We have also analyzed these initial data in terms of first-order kinetics. The first-order plots that correspond to the data in Figure 12 are shown in Figure 13. Again, the data are linear over the limited range given. Due to the extremely fast cure rates and the method that was used to cure the materials, the data were not accurate enough to obtain activation energies from the first-order rate constants. The necessity of measuring cure times as short as 15 s required using a hot plate from which the samples could be removed quickly. Although the temperature of the hot plate remained constant at a given temperature, we found that the actual temperature could be different from the

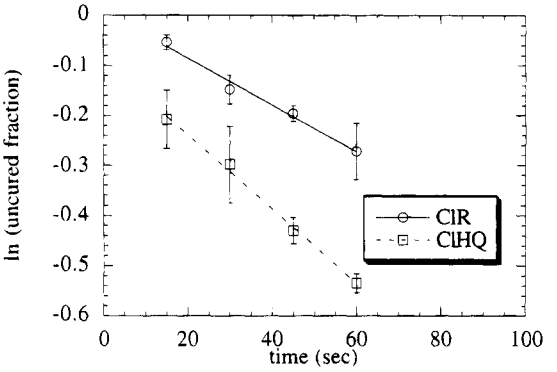

Figure 13. First-order plot for ClR and ClHQ cured at 190 °C corresponding to the data in Figure 12.

desired temperature by as much as 2 °C. Thus, comparisons at a given temperature are valid, since those samples were prepared at the same time, but comparisons between different temperatures are not accurate due to the uncertainty of the actual temperatures. This error in the temperature measurement precludes a quantitative discussion of the change in cure rates with temperature.

The initial rates and first-order rate constants are given in Tables 4 and 5, respectively. Although in some cases the error is somewhat large, the general trend for the methyl- and chloro-substituted thermosets shows that the liquid-crystalline materials cure faster than the isotropic materials for curing temperatures of 200 °C and less. The increase in rate can be quite large, ranging from 35% to 126%. As would be expected, the rates for all materials increase as a function of temperature. Above 200 °C the difference in rates between nematic and isotropic phases disappears. This is because the cure rate is so fast that the thermosets are already 60% cured after the first two data points (30 s). At these rates it is not possible to measure any difference between the two.

The rate enhancement for the methoxy-substituted thermosets is not as great. Reference to Figure 7 shows that MeOHQ is biphasic over the course of the cure. Although we cannot explain this biphasic behavior (see previous section), the effect of the biphase manifests itself in the cure rate. Since some material is curing in the isotropic phase and some is curing in the nematic phase, the average cure rate measured is between the rates for the pure phases.

Conclusions

We have synthesized a series of aromatic bisacetylene thermosets. Depending on the central aromatic group and the substituents, these thermosets can show either no melting, a crystal-to-nematic melting, or a crystal-to-isotropic melting. Changes in conformation due to substituents cannot fully explain the observed phase behavior. A combination of steric and electronic effects is likely to account for the phase behavior, confirming the results seen in previous investigations. We have also found that for one material which shows both a melting and a clearing point, the phase behavior depends on cure history. Thus, the behavior of this thermoset follows a general phase diagram for liquid-crystal thermosets that we have reported previously.

We have also measured the curing kinetics quantitatively using Raman spectroscopy. We have conclu-

Table 4. Initial Cure Rates (%/s)

curing temp (°C)[a]	ClR	ClHQ	%Δ[c]	MeOR	MeOHQ	%Δ[c]	MR	MHQ	%Δ[c]
180				0.23 ± 0.04	0.30 ± 0.04	30.4	0.26 ± 0.10	0.39 ± 0.12	50.0
185				0.28 ± 0.04	0.34 ± 0.05	21.4	0.28 ± 0.04	0.42 ± 0.11	50.0
190	0.40 ± 0.05[b]	0.66 ± 0.17	65.0	0.43 ± 0.02	0.56 ± 0.05	30.2	0.46 ± 0.06	0.62 ± 0.20	34.8
195	0.42 ± 0.09	0.95 ± 0.18	126.2	0.46 ± 0.03	0.53 ± 0.10	15.2	0.43 ± 0.05	0.76 ± 0.17	76.7
200	0.54 ± 0.12	0.89 ± 0.22	64.8	0.70 ± 0.16	0.86 ± 0.18	22.9	0.81 ± 0.09	1.15 ± 0.17	42.0
205	0.89 ± 0.10	1.06 ± 0.35	19.1	0.77 ± 0.12	0.80 ± 0.13	3.9	0.78 ± 0.002	1.10 ± 0.31	41.0
210	1.00 ± 0.21	1.93 ± 0.20	93.0	1.37 ± 0.40	1.54 ± 0.17	12.4	1.36 ± 0.09	1.75 ± 0.42	28.7
220	1.95 ± 0.12	2.30 ± 2.27	17.9	2.06 ± 0.00	1.99 ± 0.59	−3.4	2.11 ± 0.21	2.18 ± 0.82	3.3

[a] Estimated error in the temperature is ±2 °C. See text for discussion. [b] Errors are based on the linear regression fit and represent the 95% confidence limit. [c] %Δ is the increase in rate of the hydroquinone-based thermoset over the resorcinol-based thermoset.

Table 5. First-Order Rate Constants ($k_1 \times 10^3$ (s^{-1}))

curing temp (°C)[a]	ClR	ClHQ	%Δ[c]	MeOR	MeOHQ	%Δ[c]	MR	MHQ	%Δ[c]
180				2.7 ± 0.7	3.4 ± 0.5	25.9	2.8 ± 1.5	4.5 ± 1.7	60.7
185				3.1 ± 0.6	3.9 ± 0.6	25.8	3.1 ± 0.6	5.0 ± 1.6	61.3
190	4.7 ± 0.8[b]	7.4 ± 0.7	57.4	5.1 ± 0.3	7.0 ± 1.2	37.3	5.5 ± 1.3	6.6 ± 1.7	20.0
195	4.7 ± 1.4	13.9 ± 2.0	195.7	5.5 ± 0.9	6.4 ± 2.1	16.4	5.1 ± 1.1	9.8 ± 3.0	92.2
200	7.5 ± 1.6	12.2 ± 3.8	62.7	8.9 ± 42.0	12.0 ± 2.8	34.8	12.6 ± 3.4	16.6 ± 1.5	31.7
205	14.6 ± 3.4	15.7 ± 4.2	7.5	11.1 ± 2.6	11.3 ± 3.1	1.8	9.7 ± 0.6	11.9 ± 2.0	22.7

[a] Estimated error in the temperature is ±2 °C. See text for discussion. [b] Errors are based on the linear regression fit and represent the 95% confidence limit. [c] %Δ is the increase in rate of the hydroquinone-based thermoset over the resorcinol-based thermoset.

sively shown that the cure rate depends on the phase in which cure occurs. Curing occurs at the fastest rate in the nematic phase, at the slowest rate in the isotropic phase and at an intermediate rate in a biphasic material. Although the overall cure rates for this system are extremely fast (0.5 to 2% cure/s), this result may have significance for manufacturing throughput in slower curing systems or in processes where fast reacting systems are desirable, such as RIM.

Several other investigators have described the properties of LCTs, showing that oriented LCTs can exhibit an anisotropic coefficient of thermal expansion.[17,18] We are currently working to understand the properties of LCTs, especially their use in composite materials. We have described the preliminary results of our use of LCTs for the formation of molecular composites;[35] further details will be described in a future publication.

Acknowledgment. This work was supported by Laboratory Directed Research and Development Funding of the Los Alamos National Laboratory which is supported by the United States Department of Energy under Contract W-7405-ENG-36 to the University of California.

(35) Benicewicz, B. C.; Douglas, E. P.; Hjelm, R. P. In *Liquid Crystalline Polymers*; Carfagna, C., Ed.; Pergamon Press: New York, 1993; p 87.